

# Entropy growth during free expansion of an ideal gas

Subhadip Chakraborti<sup>1</sup>, Abhishek Dhar<sup>1</sup>, Sheldon Goldstein<sup>2</sup>, Anupam Kundu<sup>1</sup> and Joel L. Lebowitz<sup>2</sup>  
<sup>1</sup>International Centre for Theoretical Sciences, Tata Institute of Fundamental Research, Bengaluru 560089, India and  
<sup>2</sup>Departments of Mathematics and Physics, Hill Center, Rutgers, The State University of New Jersey,  
110 Frelinghuysen Road, Piscataway, New Jersey 08854-8019, USA

(Dated: March 13, 2022)

To illustrate Boltzmann’s construction of an entropy function that is defined for a single microstate of a system, we present here the simple example of the free expansion of a one dimensional gas of hard point particles. The construction requires one to define macrostates, corresponding to macroscopic observables. We discuss two different choices, both of which yield the thermodynamic entropy when the gas is in equilibrium. We show that during the free expansion process, both the entropies converge to the equilibrium value at long times. The rate of growth of entropy, for the two choice of macrostates, depends on the coarse graining used to define them, with different limiting behaviour as the coarse graining gets finer. We also find that for only one of the two choices is the entropy a monotonically increasing function of time. Our system is non-ergodic, non-chaotic and essentially non-interacting; our results thus illustrate that these concepts are not very relevant for the question of irreversibility and entropy increase. Rather, the notions of typicality, large numbers and coarse-graining are the important factors. We demonstrate these ideas through extensive simulations as well as analytic results.

## I. INTRODUCTION

According to the second law of thermodynamics, any spontaneous change in an isolated system leads to an increase of the thermodynamic entropy,  $S$  (as defined by Clausius). The second law thus provides in a sense an arrow of time and quantifies the irreversibility that we observe in everyday physical phenomena. Understanding how such irreversibility emerges from the microscopic reversible Newtonian dynamics of a many-particle system was the remarkable achievement of Boltzmann. He pointed out the key idea that the observed irreversibility was the typical macroscopic behaviour, that becomes a certainty when we take the system size truly macroscopic. Boltzmann also provided a clear prescription for the construction of an entropy function (which we denote as  $S_B$ ) that is defined for a *single* microstate of a system and uses the idea of a macroscopic description of a system (macrostates). This entropy function is well defined even for a system out of equilibrium and becomes equivalent to the thermodynamic entropy for a system in equilibrium.

The deep and somewhat subtle ideas of Boltzmann [1] have been widely discussed [2–5] and clarified in recent work [6–9]. We mention here a particularly relevant quote from Ref. [10]: *Time-asymmetric behavior as embodied in the second law of thermodynamics is observed in individual macroscopic systems. It can be understood as arising naturally from time-symmetric microscopic laws when account is taken of a) the great disparity between microscopic and macroscopic sizes, b) initial conditions, and c) that what we observe are “typical” behaviors — not all imaginable ones. Common alternate explanations, such as those based on equating irreversible macroscopic behavior with ergodic or mixing properties of ensembles (probability distributions) already present for chaotic dynamical systems having only a few degrees of freedom or on the impossibility of having a truly isolated system, are*

*either unnecessary, misguided or misleading.*

We also note here the important difference between Boltzmann’s entropy function  $S_B$  and the one due to Gibbs (which we denote by  $S_G$ ) as discussed recently in [9]. While the former is defined for a single microstate and can change with time under Hamiltonian evolution, Gibbs entropy is defined only for ensembles and does not evolve under Hamiltonian evolution. The article [9] explains the concept of macrostates for the macroscopic description of systems with large numbers of particles and discusses different choices of macrostates and corresponding entropy functions. The present work is an attempt to provide a numerical demonstration of some of the ideas presented in [9] through the simple example of the free expansion of a classical ideal gas in one dimension. Boltzmann’s ideas also appear in recent discussions of thermalization in isolated quantum systems [11, 12].

Our microscopic model is a gas of  $N (\gg 1)$  hard point particles of equal mass confined to move inside a box of length  $L$ . Initially the gas is in thermal equilibrium (to be defined more precisely later) and confined, by a partitioning wall, to the left half of the box. We consider its subsequent evolution on removal of the partition. In our work we consider two distinct (families of) macroscopic observables. For the first, we consider a coarse graining of the single particle phase space  $\{\mu \equiv (x, v)\}$  and look at the distribution  $f(x, v, t)$  of particles in this space. This leads to a definition of  $S_B$ , that we refer to as  $S_B^f$ , that is essentially just the negative of the Boltzmann  $H$ -function. The second macroscopic description is given by the three locally conserved fields  $U = \{\rho(x, t), p(x, t), e(x, t)\}$  corresponding to mass, momentum and energy — defined using a spatial coarse-graining. The Boltzmann entropy corresponding to  $U$  will be referred to as  $S_B^U$ . For non-interacting systems in equilibrium both  $S_B^f$  and  $S_B^U$  correspond to the thermodynamic entropy. One expects that, for dilute weakly interacting systems, the out-of-equilibrium behaviour of both these entropies should be

similar and should increase monotonically with time.

We study the time evolution of the two choices of macrostates,  $f$  and  $U$ , and the associated entropies,  $S_B^f, S_B^U$ . One of our main findings is that for typical initial conditions corresponding to the gas being in equilibrium in the left half of the box, the second choice of entropy has a monotonic increase with time during free expansion. We provide a clear explanation and point out subtleties that arise in numerical verifications with finite systems and finite phase-space discretizations. We also discuss other initial conditions where the monotonic increase of entropy is not observed though the final value of entropy (for  $S_B^U$ ) could still saturate to the expected equilibrium value. The simplicity of the model allows us to perform highly accurate simulations with large number of particles (of order  $10^7$ ) and compute both mean distributions (averaged over initial ensembles) as well as empirical ones (with single realizations). Some exact results are also obtained. Our model is effectively a non-interacting system and so our work also shows that a demonstration of irreversibility does not require the system to have properties such as chaos, ergodicity and mixing.

We point to some of the earlier studies related to this issue. The evolution of the  $H$ -function was studied numerically in fluid models [13–15] and in lattice gas models [16]. Falcioni et al [17] looked at the evolution of  $S_B^f$  in a many-particle system evolving via a symplectic map and looked at the effect of interactions and chaos and also pointed to subtleties associated with the coarse-graining procedure. It was pointed out in [18, 19] that for dense liquids, one is not assured of a monotonic increase of the  $H$ -function version of  $S_B^f$ , which does not take the total energy  $E$  into account; thus it was argued that one should consider a macrostate specified by both the single particle distribution function  $f(x, v, t)$  and the energy  $E$ —or better still, the energy profile  $e(x, t)$ . A numerical verification of this proposal was obtained in [20].

The one dimensional gas of equal mass hard point particles and hard rods was extensively studied earlier as one of the tractable models where dynamical properties can be obtained analytically and where the question of entropy increase has been investigated. Some of the interesting questions addressed concern dynamical correlations and the evolution of the single particle distribution function [21–27]. The Euler hydrodynamic equations for the hard rod system were first obtained in [28] and have more recently been discussed in [29] as an example of an interacting integrable model, where it is also shown that there are dissipative Navier-Stokes corrections. In [29] an entropy function is defined that, in equilibrium, is equal to the hard rod thermodynamic entropy (when it equals  $S_B^U$ ), but in general differs from both  $S_B^f$  and  $S_B^U$  except when the rods become points. For the case of a domain wall initial condition, it was then shown that the entropy does not change at the level of the Euler equations but the dissipation terms lead to a positive entropy production. Interestingly, the dissipation terms vanish when one goes from rods to point particles. The effect of integrability-breaking on entropy growth was studied in

[30] for hard rods in a harmonic trap.

The main aim of the present paper is to demonstrate that even for a system as simple as the one-dimensional hard point gas (HPG), Boltzmann’s central idea concerning thermalization works. Indeed the HPG is perhaps the simplest. In this paper, we address the following issues in the context of the HPG:

- Checking typicality in the evolution of the macroscopic quantities such as the single particle distribution function  $f(x, v, t)$ , density field  $\rho(x, t)$ , velocity field  $v(x, t)$ , and temperature field  $T(x, t)$  as the system evolves in a single typical microscopic configuration.
- Exploring how the evolution of entropy depends on the choice of macrostates.
- Investigating how typicality of initial conditions gets manifested in the evolution of the entropies for both choices of macrostates.
- Understanding the effect of various numerical issues, related to coarse graining and finite system sizes, on the evolution of the different entropies.
- Understanding the source of entropy production in the case when the entropy increases.

The plan of the paper is as follows. In Sec. II we define the precise model, the different definitions of entropy that are studied and the choices of macrostates. In Sec. III we present our numerical results on the evolution of the macroscopic fields and the entropy functions for the two different choices of macrovariables. In Sec. IV we study how these macrovariables and the associated (Boltzmann) entropies evolve with time for non-equilibrium initial conditions. We present an analysis of the results in Sec. V, including a discussion based on the “hydrodynamic” equations for the macroscopic fields. A geometric picture of the dynamics in phase space is provided in Sec. VI and we conclude with a discussion in Sec. VII. Some exact results for the evolution of the macroscopic fields in the case of the hard particle gas are presented in Appendix A.

## II. BOLTZMANN’S ENTROPY, DEFINITION OF THE MICROSCOPIC MODEL AND CHOICE OF MACROSTATES

### A. Boltzmann’s entropy

Though the relevant formalism is quite general, we restrict ourselves to the case of a system in one dimension. Let us consider an isolated classical system of  $N(\gg 1)$  particles, each of mass  $m$ , confined to move inside a *one dimensional* box of length  $L$ . The microstate of the system, denoted by  $X$ , is specified by the positions  $x_i$  and momenta  $p_i$ , with  $i = 1, 2, \dots, N$ , *i.e.*,  $X = (x_1, x_2, \dots, x_N, p_1, p_2, \dots, p_N)$ . The system is

described by a Hamiltonian  $H(X)$  and evolves in a  $2N$  dimensional phase space, according to the Hamiltonian dynamics:

$$\dot{x}_i = \partial H / \partial p_i, \dot{p}_i = -\partial H / \partial x_i, \quad (1)$$

for  $i = 1, 2, \dots, N$ . If we consider an ensemble of points in phase space, the corresponding distribution function,  $\varrho(X, t)$ , evolves through the Liouville equation

$$\partial \varrho / \partial t = \{H, \varrho\}, \quad (2)$$

where  $\{A(X), B(X)\} = \sum_{i=1}^N \partial A / \partial x_i \partial B / \partial p_i - \partial A / \partial p_i \partial B / \partial x_i$  denotes the Poisson bracket for any two phase space functions.

We now consider the macroscopic or ‘coarse-grained’ description. A simple example of such a description is provided by the macrovariable  $n_L$  which gives the total number of particles in the left half of the box. Clearly, this is a function of the microstate  $X$  and we can write  $n_L(t) = M(X(t))$ , with  $M(X) = n_L(X)$ . Also we note that there are a large number of microstates which would give the same value of  $n_L(t)$ . In general we can describe a macrostate by specifying a set of macrovariables  $M(X) = \{M_1(X), M_2(X), \dots, M_n(X)\}$ , with resolution  $\Delta M = \{\Delta M_j\}$  [9]. Typically we expect this to be a coarse-grained description in the sense that many different  $X$  correspond to the same  $M$ . We will give specific examples of such macrostates later in this section.

Boltzmann’s insight was to associate to each microscopic state  $X$  an entropy through the macrostate  $M = M(X)$  it realises, with [6, 8, 9, 31]

$$S_B(M) = \ln |\Gamma_M|, \quad (3)$$

where we have set Boltzmann’s constant  $k_B = 1$  and

$$|\Gamma_M| = \int \prod_{i=1}^N dx_i dp_i \mathbb{1}[M < M(X) < M + \Delta M] \quad (4)$$

is the volume in phase space of all points  $X$  with  $M(X)$  between  $M$  and  $(M + \Delta M)$  and  $\mathbb{1}$  represents the indicator function. As the system evolves under the Hamiltonian dynamics, the microstate is given by  $X(t)$  while the macrostate evolves as  $M(t) = M[X(t)]$  and correspondingly the Boltzmann entropy as  $S_B(t) = S_B[M(t)]$ . Boltzmann argued that for an isolated system starting from a microstate corresponding to a low entropy  $S_B(0)$ , the system evolves in such a way that  $S_B(t)$  ‘typically’ increases for macroscopic systems even though the microscopic evolution is completely time-reversal symmetric.

Among all possible macrostates of a system there are two very important ones: the equilibrium macrostate  $M_{eq}$  and the initial macrostate  $M_{ini}$ . The entropy of the initial macrostate  $S_B(t=0) = S_B(M_{ini})$  is low by assumption. On the other hand, the macro-region  $\Gamma_{M_{eq}}$  is overwhelmingly large compared to other macro-regions associated to other macrostates. It is so large that it contains most of the phase space volume of  $\Gamma_E$ , an energy shell, assumed to contain all the macrostates  $M$ .

More precisely, for large  $N$ , the ratio of their volumes  $|\Gamma_{M_{eq}}|/|\Gamma_E| \approx 1 - e^{-cN}$  where  $c$  is a positive constant [31–33]. This property corresponds to equilibrium because the system should stay in (or near)  $\Gamma_{M_{eq}}$  for long times, consistent with the observed stationarity in thermodynamic equilibrium.

Since  $\Gamma_{M_{eq}}$  takes up almost all the volume of  $\Gamma_E$ , when the system starts from a microstate  $X$  belonging to a non-equilibrium macrostate  $M_{ini}$  such that  $S_B(M_{ini}) \ll S_B(M_{eq})$ , its microscopic dynamics would ‘typically’ take the microstate to regions of larger entropy  $S_B$ , unless the dynamics and/or the initial state  $X$  are ridiculously special [34]. Hence we expect the quantity  $S_B(M)$  to increase for the majority (in fact the overwhelming majority) of microstates in  $\Gamma_{M_{ini}}$  except for a few whose total volume with respect to  $\Gamma_{M_{ini}}$  goes to zero in the  $N \rightarrow \infty$  limit. Because of this expectation one can make direct connection between  $S_B(M_{eq})$  and  $S$  (the thermodynamic entropy) in an equilibrium state as suggested by Boltzmann. For an isolated system in equilibrium with energy  $E$ , volume  $V$  and  $N$  particles [8]

$$S(E, V, N) \simeq S_B(M_{eq}(E, V, N)), \quad \text{for large } N. \quad (5)$$

We briefly comment here on why Gibbs’ definition of entropy cannot be used in the nonequilibrium situation. We recall first that the Gibbs entropy of an equilibrium ensemble  $\varrho_{eq}$  is defined as

$$S_G[\varrho_{eq}(X)] = - \int \prod_{i=1}^N dx_i dp_i \varrho_{eq}(X) \ln \varrho_{eq}(X), \quad (6)$$

and this can be identified with the thermodynamic entropy  $S$ . Extending this definition to the non-equilibrium situation described by an evolving ensemble  $\varrho_t(X)$  one obtains the corresponding Gibbs entropy  $S_G(t) = S_G[\varrho_t(X)]$ . However, we note that the volume preserving Liouville dynamics in Eq. (2) ensures that this entropy does not change with time, i.e.,  $dS_G(t)/dt = 0$ .

## B. Definition of the microscopic model and choices of macrostates

Our model of the ideal gas consists of  $N$  hard point particles interacting via perfectly elastic collisions and confined in a one dimensional box of size  $L$ . During collisions, particles cannot cross each other and thus their initial order is preserved. The Hamiltonian of the system  $H = \sum_{j=1}^N p_j^2/2$  consists of only kinetic energy and we set the mass of all particles to one. The particles are ordered satisfying  $0 \leq x_1 \leq x_2 \dots x_N \leq L$ . The collisions conserve energy and momentum and this means that two colliding particles simply exchange their velocities when they collide. At the boundaries the particles that collide with the walls are reflected with their velocities reversed. As a consequence, by exchanging the label of two particles at the time of collision, one can consider the system effectively as non-interacting, as noted

by Jepsen [22]. This mapping to a non-interacting gas allows one to obtain many analytic results for this system [24–27]. Since the mass of each the particles is unity, the momentum of each particle is equal to its velocity *i.e.*  $p_j = v_j$ ,  $j = 1, 2, \dots, N$ .

We now describe the two families of macrovariables that we will consider in this study.

**Choice I — The distribution of particles in the single-particle phase space:** We consider  $\mu$ -space  $\{(x, v)\}$  and divide it into cells  $\Delta_\alpha$ , each of size  $|\Delta_\alpha| = \Delta x \Delta v$ . For a given microstate  $X = \{x_i, v_i\}$  we specify the number of particles  $N_\alpha$  in each cell. We then obtain the particle number density in each cell:

$$f_\alpha = \frac{N_\alpha}{|\Delta_\alpha|}. \quad (7)$$

This satisfies the normalization  $\sum_\alpha f_\alpha |\Delta_\alpha| = N$ . The set  $\{f_\alpha\}$  specifies our first family of macrovariables, with its corresponding macrostates. The “number” of microstates (volume) for a given specification of  $\{N_\alpha\}$  is given by  $|\Gamma_M| = \prod_\alpha [|\Delta_\alpha|^{N_\alpha} / N_\alpha!]$ . Thus, with  $S_B^f = \ln |\Gamma_M|$ , we have for large  $N$  the entropy per particle

$$s_B^f = S_B^f / N = -\frac{1}{N} \sum_\alpha |\Delta_\alpha| f_\alpha \ln f_\alpha, \quad (8)$$

up to an additive constant. For large  $N$ , corresponding to  $f_\alpha$  defined for a given microstate  $X = \{x_i, v_i\}$ , one can associate a smooth function  $f(x, v, t)$  such that  $N_\alpha = \int_{x, v \in \Delta_\alpha} dx dv f(x, v, t)$  and  $\int dx dv f(x, v, t) = N$ . The Eq. (8) then becomes

$$s_B^f(t) \approx -\frac{1}{N} \int dx dv f(x, v, t) \ln f(x, v, t), \quad (9)$$

up to an additive constant.

In the large  $N$ , small grid size limit, the function  $\tilde{f} = \lim_{\Delta x \rightarrow 0, \Delta v \rightarrow 0} \lim_{N \rightarrow \infty} f/N$  satisfies the equation

$$\partial_t \tilde{f} + v \partial_x \tilde{f} = 0, \quad (10)$$

using which it follows that it’s associated “entropy”

$$s_B^f(t) = - \int dx dv \tilde{f}(x, v, t) \ln \tilde{f}(x, v, t), \quad (11)$$

obeys  $ds_B^f(t)/dt = 0$ . Thus it would seem that there is no entropy increase in the large  $N$  limit. However, such a conclusion would be misleading and in fact in apparent contradiction to our numerical findings in Sec. III. For any finite  $N$ , no matter how large, and fixed grid size  $|\Delta_\alpha|$  the exact  $s_B^f$ , or its approximation on the right hand side of Eq. (8), will typically increase (if initially its value is not at its maximum) over time. For  $N$  large and  $|\Delta_\alpha|$  small, significant increase may not begin for a very long time (the time at which  $\tilde{f}(x, v, t)$  develops structure on the scale  $|\Delta_\alpha|$ ), a reflection of the fact that the limiting entropy (11) does not change with time.

To get a handle on the behavior of  $s_B^f$  we also consider, for a finite number of particles, an average over initial

microscopic configurations chosen from the phase space distribution  $\varrho_0(\{x_i(0), v_i(0)\})$ :

$$F(x, v, t) = \sum_{i=1}^N \langle \delta(x_i - x) \delta(v_i - v) \rangle, \quad (12)$$

which we note is the single-particle marginal obtained from the Gibbs distribution or any other one for the full phase space density  $\varrho_t(\{x_i, v_i\})$  with initial distribution  $\varrho_0$ . For our equal mass gas  $F(x, v, t)$  obeys Eq. (10) and can be computed analytically as shown in Appendix. A. Such an analytical computation is possible since our model can be mapped to a gas of non-interacting particles (Jepsen mapping [22]) and the quantities of interest do not depend on the particle labels. Finally, we can also define a coarse grained quantity corresponding to a partition of the  $\mu$ -space as

$$F_\alpha = \frac{1}{|\Delta_\alpha|} \int_{x, v \in \Delta_\alpha} dx dv F(x, v, t). \quad (13)$$

Corresponding to this we can define the following entropy per particle

$$s^F = -\frac{1}{N} \sum_\alpha |\Delta_\alpha| F_\alpha \ln F_\alpha. \quad (14)$$

Note that this has a similar form as Eq. (8); however, here we have used mean distributions instead of the empirical distributions used there. These will in fact typically be more or less the same, a consequence of the law of large numbers.

**Choice II - The spatial distribution of mass, momentum and energy:** We divide the box  $(0, L)$  into  $K$  cells  $\delta_a$ ,  $a = 1, 2, \dots, K$ , each of size  $\ell = L/K$ . For a given microscopic configuration  $X$ , let  $N_a$  be the number of particles in cell  $\delta_a$  and let  $P_a$  and  $E_a$  be the total momentum and total energy of these particles. In this case the macrostate is defined by these set of conserved quantities  $U = \{N_a, P_a, E_a\}$  and we obtain the Boltzmann entropy  $S_B^U = \ln |\Gamma_U|$  where  $|\Gamma_U|$  is the volume of the phase space region  $\Gamma_U$  corresponding to the macrostate  $U$ . For large  $N$  this entropy per particle attains the form

$$s_B^U = \frac{S_B^U}{N} = \frac{1}{N} \sum_a \rho_a \ell s(\rho_a, \epsilon_a), \quad (15)$$

where  $s(\rho_a, \epsilon_a)$  is the ideal gas entropy per particle for density  $\rho_a = N_a/\ell$  and internal energy density  $\epsilon_a = [E_a - P_a^2/(2N_a)]/\ell = e_a - p_a^2/(2\rho_a)$ , with  $p_a = P_a/\ell$ ,  $e_a = E_a/\ell$  being the momentum density and total energy density respectively. This is given explicitly (up to additive constant terms) by [35]

$$s(\rho, \epsilon) = \left[ \frac{1}{2} \ln \left( \frac{\epsilon}{\rho} \right) - \ln \rho \right]. \quad (16)$$

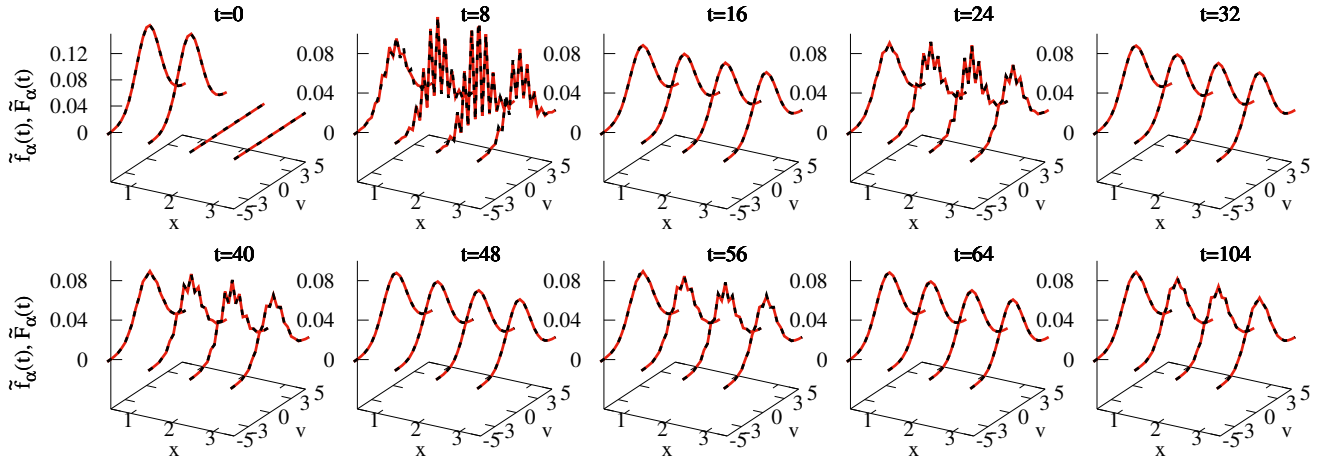


FIG. 1. Plot of evolution of the empirical particle density  $\tilde{f}_\alpha(t) = f_\alpha(t)/N$  (black dashed lines) starting from a single initial microscopic configuration in the two-dimensional  $\mu$ -space for grid size  $\Delta x = \Delta v = 0.5$  and  $N = 10^7$ ,  $L = 4$ . In the single initial configuration, the positions of the particles are distributed uniformly between  $(0, L/2)$  and the velocities are drawn from the Maxwell distribution given by Eq. (17) with canonical temperature  $T_0 = 2.5$ . We observe that  $\tilde{f}_\alpha(t)$  approaches towards its equilibrium form at large times, however the convergence is oscillatory as can be seen from the recurrences at times  $t = 16, 32, 48, 64$  to very close to the equilibrium form. The evolution is also compared with the analytical result for the averaged single particle distribution  $\tilde{F}_\alpha = F_\alpha(t)/N$  from Eqs. (13) and (A8) which is obtained after averaging over initial configurations chosen from uniform position distribution over  $(0, L/2)$  and Maxwell velocity distribution at temperature  $T_0 = 2.5$  (this is the equilibrium state in the left half of the box). The good agreement between  $\tilde{f}_\alpha(t)$  and  $\tilde{F}_\alpha(t)$  is a consequence of typicality.

### III. NUMERICAL RESULTS FOR EVOLUTION OF MACROSTATES AND ENTROPY INCREASE

#### A. Choice I of the macrovariables

We consider  $N = 10^7$  particles initially uniformly distributed in the left half  $(0, L/2)$  of the box with box size  $L = 4$ . For our hard point particle system with no interactions, the choice of system size  $L$  is inconsequential and hence we arbitrarily set  $L = 4$ . Since we keep the system length fixed, changing  $N$  corresponds to changing the density in our system. There is no upper bound to the density since there is no effective interaction between the particles. In real systems the number of particles would scale with the volume. The initial velocities are drawn from the Maxwell distribution given by

$$g_{\text{eq}}(v, T_0) = \left( \frac{1}{2\pi T_0} \right)^{1/2} \exp \left( -\frac{v^2}{2T_0} \right), \quad (17)$$

with temperature  $T_0 = 2.5$ . This is thus the canonical ensemble corresponding to the equilibrium macrostate with particles in the left half of the box. We thus choose a *single random realization* from this canonical ensemble as our initial microstate.

We divide the  $\mu$ -space ( $x$ - $v$  space) of the system into grids of size  $\Delta x = \Delta v = 0.5$  and calculate the evolution of the empirical single particle density  $f_\alpha$  given by Eq. (7) by performing microscopic simulations. In Fig. 1 we plot  $\tilde{f}_\alpha = f_\alpha(t)/N$  at different points  $x_\alpha, v_\alpha$  in  $\mu$ -space and at different times. We observe that  $\tilde{f}_\alpha(t)$  ap-

proaches its equilibrium form non-monotonically in time with near-recurrences to the equilibrium distribution. At large times, the  $\tilde{f}_\alpha(t)$  finally reaches the equilibrium form where particles are uniformly distributed between  $(0, L)$  and velocities are Maxwellian with temperature  $T_0 = 2.5$ . We also compare the empirical  $\tilde{f}_\alpha(t)$  (black dashed lines) and mean distribution  $\tilde{F}_\alpha(t)$  (red solid lines) calculated for grid size  $\Delta x = \Delta v = 0.5$  at different times. The mean distribution  $F_\alpha(t)$  is computed analytically from Eqs. (13) and (A8).

We find good agreement between the empirical density  $\tilde{f}_\alpha(t)$  and the mean distribution  $\tilde{F}_\alpha(t)$  — a consequence of the typicality implied by the law of large numbers for this non-interacting model. We have verified that this agreement is also valid when we choose the initial random configuration from a microcanonical distribution with energy per particle given by  $T_0/2$ . We show the evolution of the corresponding empirical entropy  $s_B^f(t)$  [given by (8)] during free expansion in Fig. 2 for the same random single realization and parameters as in Fig. 1. We plot  $s_B^f(t)$  for different grid sizes  $|\Delta_\alpha| = \Delta x \Delta v$  by keeping  $\Delta x$  fixed and varying  $\Delta v$ . The solid lines correspond to the entropy  $s^F(t)$  [given by (14)] calculated from the exact expression for the mean distribution  $F(x, v, t)$ . We observe that there is very good agreement between  $s_B^f$  and  $s^F$ , as expected. Both the entropies grow non-monotonically with time and in fact exhibit oscillations in time with a period  $2L/\Delta v$ ; these eventually die and the entropy saturates to its equilibrium value.

Note that these oscillations were also seen in the re-

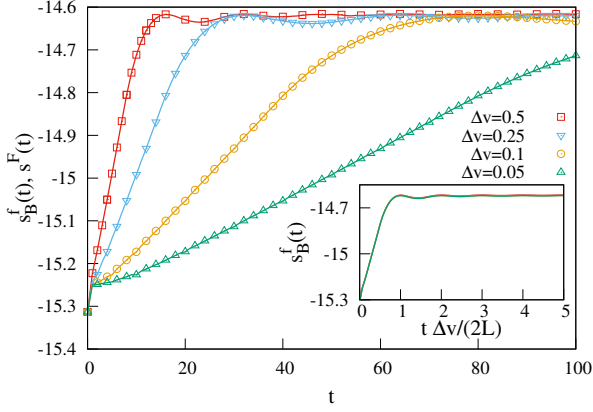


FIG. 2. A comparison between  $s_B^f(t)$  obtained from simulation of a single realization, and  $s_B^F(t)$  obtained after an ensemble average, plotted as a function of time during free expansion. For evaluating  $s_B^f(t)$  we use the same single initial condition used in Fig. 1 for  $N = 10^7$  in a box of size  $L = 4$ . We compute  $s_B^f(t)$  for different grid sizes  $|\Delta_\alpha| = \Delta x \Delta v$  by keeping  $\Delta x = 0.5$  fixed and varying  $\Delta v = 0.5$  (red empty squares), 0.25 (blue empty inverted triangles), 0.1 (yellow empty circles), and 0.05 (green empty triangles). The solid lines are  $s_B^F(t)$  obtained analytically from Eq. (14) for  $T_0 = 2.5$ . We again observe excellent agreement between  $s_B^f(t)$  and  $s_B^F(t)$  and notice that they both eventually increase and saturate to the equilibrium value. However the approach to this equilibrium value is oscillatory with decaying amplitude and period  $2L/\Delta v$ . Also note that the growth rate decreases with decreasing the grid sizes  $|\Delta_\alpha|$ . Inset: Note that the entropy growth plots for different  $\Delta v$  collapse onto a single curve on scaling the time by the oscillation period.

currences in Fig. 1. The oscillation period  $2L/\Delta v$  can be understood from the fact that two particles, initially in a particular spatial bin and with velocity difference  $\Delta v$  (size of the velocity grid), will meet again (possibly in a different bin) after time  $2L/\Delta v$ . Since the spatial distribution has almost become homogeneous, it is then assured that the velocity distribution will show recurrence at these time period.

We also observe in Fig. 2 that the entropy growth rate decreases with decreasing  $\Delta v$ . In other words, at any fixed time, with decreasing  $\Delta v$  one observes a correspondingly lower entropy increase. This behaviour is consistent with the discussion after Eq. (10). The final increase of entropy, however, appears to be always equal to  $\ln(2)$ . Furthermore we show in the inset of Fig. 2 that plots of the entropy growth for different values of  $\Delta v$  collapse to a single curve on scaling time by the oscillation period  $2L/\Delta v$ .

### B. Choice II of the macrovariables

We again start from a typical single realization with  $N = 10^7$ ,  $L = 4$  and  $T_0 = 2.5$  (the same as that used in Fig. 1). In this case we partition the box into  $K = 40$

cells each of size  $\ell = L/40 = 0.1$  and calculate the corresponding empirical density  $\rho(x, t)$ , velocity  $v(x, t) = p(x, t)/\rho(x, t)$  and energy  $e(x, t)$  fields. Suppressing the time dependence, we have that  $\rho_a = \rho(x_a)$ ,  $p_a = p(x_a)$ , and  $e_a = e(x_a)$ ,  $x_a \in \delta_a$ , with corresponding temperature field  $T(x) = 2e(x)/\rho(x) - v^2(x)$ . In Fig. 3, we plot these fields at different times. The solid lines are the analytically obtained averaged fields  $\bar{\rho}$ ,  $\bar{v}$ , and  $\bar{T}$  given by Eqs. (A9), (A11), (A13). The details of the analytical calculation of mean fields are provided in Appendix A. We find excellent agreement between the empirical and mean densities, as expected. We also find that at long times these fields converge to their equilibrium values given by the uniform fields  $\rho(x) = \rho_0$ ,  $v(x) = 0$  and  $T(x) = T_0$ . Unlike for the case of the  $f$ -macrovariable, here we do not see an oscillatory approach to the equilibrium state. In fact from the analytic results (see Appendix A) one can see that the approach to equilibrium at long times takes the form  $A(x, t) - A_{\text{eq}}(x) \sim B(x) e^{-at^2}$  with  $a = T\pi^2/(2L^2)$ , where  $A(x, t)$  can be any of the three fields  $\rho, v, T$  discussed above,  $A_{\text{eq}}(x)$  represents its equilibrium value and  $B(x)$  is some real known function. Next, we compute the empirical density field for different values of  $N$ . In Fig. 4 we plot the evolution of  $\rho(x, t)$  for the different values of  $N$  and compare them with the respective mean profiles  $\bar{\rho}(x, t)$  at different times (black dot-dashed lines). We notice that the empirical density shows fluctuations for small  $N$  which decrease for increasing  $N$ , leading to better agreement of the empirical profiles with the averaged ones.

We next insert these three fields into Eqs. (15) and (16) to obtain the intensive empirical entropy  $s_B^U(t)$ . In Fig. 5 we plot  $s_B^U(t)$  with time  $t$  for different cell sizes  $\ell$ . The solid lines correspond to theoretical computation of  $s_B^U(t)$  using the analytical expressions of the mean fields  $\bar{\rho}(x, t)$ ,  $\bar{p}(x, t)$  and  $\bar{e}(x, t)$  given in Appendix A. In this case we see that the increase of  $s_B^U(t)$  is monotonic and the entropy growth rate converges as we decrease the cell size  $\ell$ . The final increase of entropy is again equal to  $\ln(2)$ , as expected.

### IV. OTHER INITIAL CONDITIONS

So far we have considered a single typical initial condition for a macrostate in which the initial positions are uniformly distributed in  $(0, L/2)$  and the initial velocities are chosen from a (uniform) Maxwell distribution. We found that at large times the system goes to equilibrium, with the profiles of the conserved fields becoming flat and the corresponding entropy  $s_B^U(t)$  reaching a steady value. It is also interesting to study the evolution for a single initial condition, atypical for all the particles being on the left side.

To do that we first consider a single configuration of  $N = 10^7$  particles initially in the left half  $(0, L/2)$  distributed uniformly. The initial velocities of odd particles are set to  $v_0 = \sqrt{T_0}$  and that of even particles are set to  $v_0 = -\sqrt{T_0}$ , with  $T_0 = 2.5$ . Interestingly, in this case,

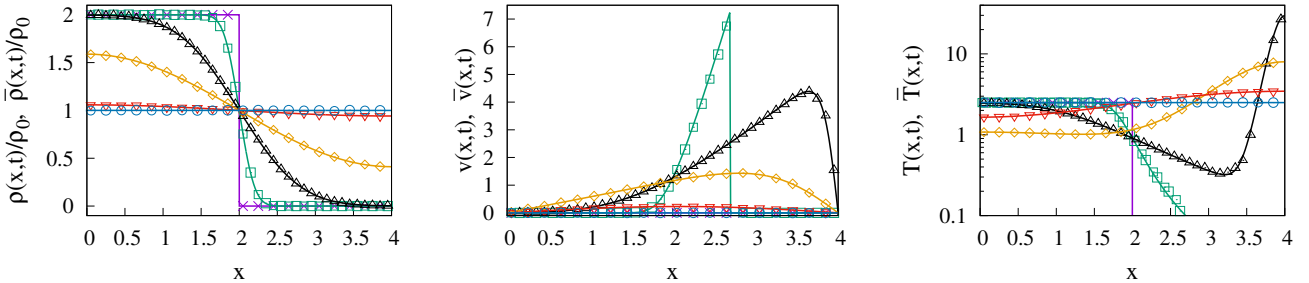


FIG. 3. Plot of the ‘typical’ spatial profiles of the three conserved fields density  $\rho(x, t)$ , velocity  $v(x, t)$ , and temperature  $T(x, t)$  at different times  $t = 0$  (magenta crosses),  $0.1$  (green empty squares),  $0.4$  (black empty triangles),  $1$  (yellow empty diamonds),  $2$  (red inverted empty triangles), and  $4$  (blue empty circles) obtained from simulation of a single configuration with  $N = 10^7$  particles. The density is normalised by the mean value  $\rho_0 = N/L$ . Initial configuration is one realization of the canonical ensemble for particles in the left half  $(0, L/2)$  with  $L = 4$ . The initial positions of the particles are distributed uniformly between  $(0, L/2)$  and the initial velocities are drawn from Maxwell distribution given by Eq. (17) with canonical temperature  $T_0 = 2.5$ . The solid lines are analytically obtained fields  $\bar{\rho}$ ,  $\bar{v} = \bar{p}/\bar{\rho}$ , and  $\bar{T}$  given by Eqs. (A9), (A11), (A13) (see Appendix A for details). The excellent agreement between the empirical densities and the mean densities once again establish typicality.

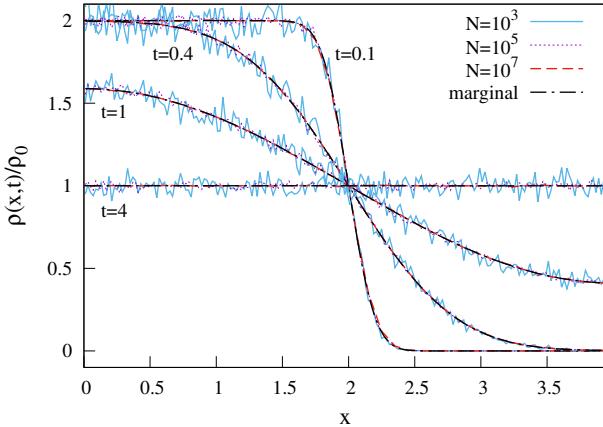


FIG. 4. Testing the dependence of typicality on the number of particles  $N$ . We plot the empirical density  $\rho(x, t)$  (normalised by  $\rho_0 = N/L$ ) for different  $N$  and at different times, along with the mean density. The agreement of the empirical profiles with the averaged ones (dashed-dotted lines) becomes better as  $N$  is increased.

each particle comes back to its original position with its original velocity periodically after a time period  $2L/\sqrt{T_0}$ . This recurrence is observed in Fig. 6, where we plot the profiles of the three conserved fields density  $\rho(x, t)$ , velocity  $v(x, t)$ , and temperature  $T(x, t)$  at different times. We note that the profiles repeat themselves after a time period  $8\tau$  with  $\tau = L/(4\sqrt{T_0})$ . Thus, unlike for the typical initial configuration in Fig. 3, for this atypical initial condition the system never settles down into an equilibrium state for either of our two choices of macrovariables. We have also looked at the evolution of the entropies  $s_B^f(t)$  and  $s_B^U(t)$  for this atypical initial configuration in Fig. 7, where we find, of course, that the entropy in both cases keeps oscillating for all time.

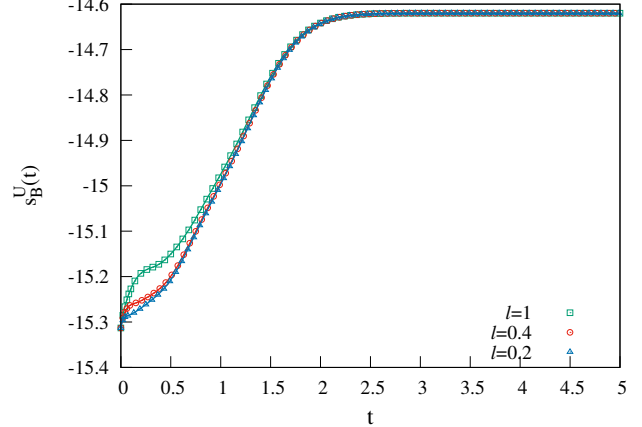


FIG. 5. Plot of entropy per particle,  $s_B^U$ , as a function of time during free expansion. Parameter values are:  $L = 4, N = 10^5, T = 2.5$ . We consider the same single initial configuration as in Fig. 1. The different plots correspond to partitions of size  $\ell = 0.2, 0.4, 1$ . Unlike in Fig. 2, here we see a monotonic increase and a convergence of the growth rate on decreasing  $\ell$ . The solid lines correspond to the mean field analytic profiles and we find very good agreement with the entropy computed from the empirical fields.

We also consider another initial microstate corresponding to an  $f$ -macrostate (choice-I) where the particles are uniformly distributed over the full box with zero momentum and with two different temperatures on the left and right half of the box, i.e., with the velocities chosen from the corresponding Maxwellians. In Fig. 8 we show the time-evolution of  $f(x, v, t)$  while Fig. 9 shows the evolution of the three fields – density, velocity and temperature. In the former case we see that the long-time form of the single particle distribution is non-thermal, *i.e.* non-Maxwellian, as demonstrated and explained in Fig. 8. On

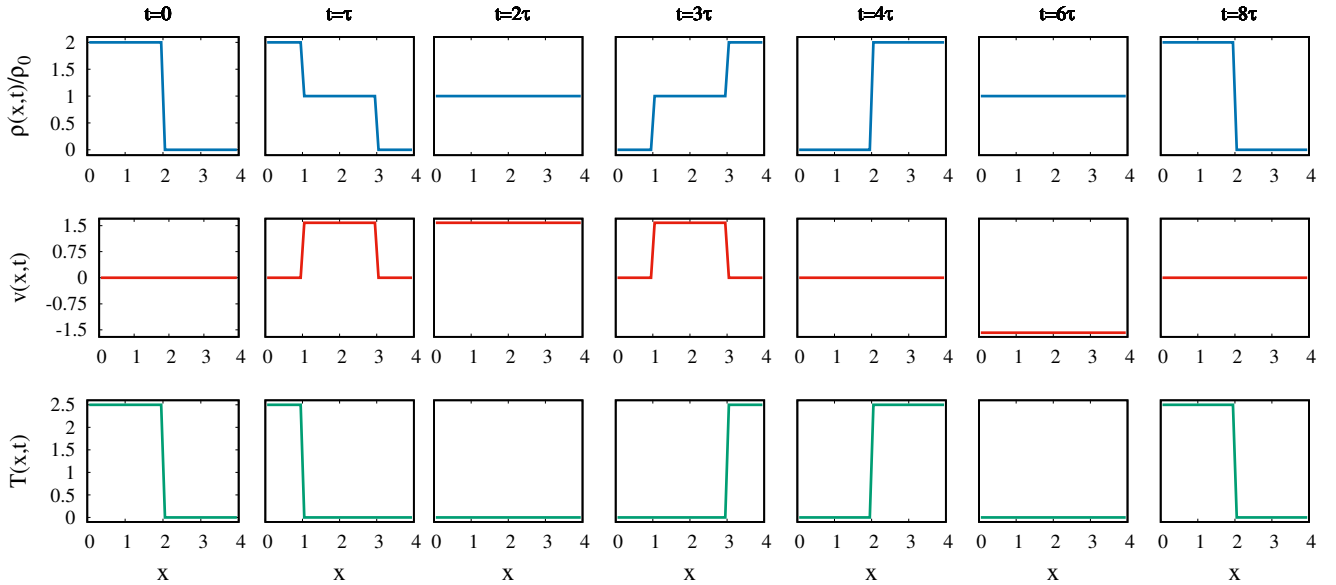


FIG. 6. Plot of the ‘atypical’ spatial profiles of the three conserved fields density  $\rho(x, t)$ , velocity  $v(x, t)$ , and temperature  $T(x, t)$  at different times obtained from simulation of a single configuration with  $N = 10^7$  particles. The initial positions of the particles are distributed uniformly between  $(0, L/2)$  with  $L = 4$ , and the initial velocities of odd particles are set  $v_0 = \sqrt{T_0}$  and of even particles are set  $v_0 = -\sqrt{T_0}$ , with  $T_0 = 2.5$ . The profiles repeat themselves after a time period  $8\tau$  with  $\tau = L/(4\sqrt{T_0})$  and thus the system does not reach an equilibrium at large time in this ‘atypical’ case. We have used grid size  $\ell = 0.1$ .

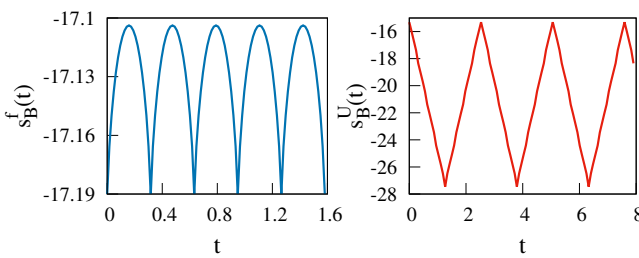


FIG. 7. Plot of  $s_B^f(t)$  and  $s_B^U(t)$  for the ‘atypical’ initial configuration and parameters considered in Fig. 6. The periodic oscillation in both cases imply that the system never reaches equilibrium. For the left figure we have used grid size  $\Delta x = \Delta v = 0.5$  and for the right figure we have used  $\ell = 0.1$ .

the other hand, the fields  $\rho(x, t)$ ,  $v(x, t)$  and  $T(x, t)$  are converging to their expected thermal equilibrium values, as shown in Fig. 9. In Fig. 10 we compare the evolution of  $s_B^f$  and  $s_B^U$  for the case where the left and right halves are initially at temperatures  $T_L = 1$  and  $T_R = 10$  respectively. We note that both  $s_B^U$  and  $s_B^f$  saturate at long times but the increase in entropy is less for  $s_B^f$ . This is because the conserved fields evolve at long times to their thermodynamic equilibrium values, with uniform density, zero momentum and temperature  $T = (T_L + T_R)/2$ , with  $s_B^U$  thus attaining the corresponding equilibrium value. On the other hand, the total velocity distribution does not evolve with time and hence remains non-Maxwellian (in fact it is the sum of two Maxwellians) at all times.

Thus  $s_B^f$  saturates to a value lower than the equilibrium one. Note that the entropy growth for both cases is non-monotonic, unlike what is seen for  $s_B^U$  for free expansion.

## V. ENTROPY INCREASE FOR $S_B^U$ AND HYDRODYNAMICS

We now explore the connection between the increase of the entropy  $S_B^U$  and the behavior of the  $U$ -macrovariables in the hydrodynamic limit. It is believed that the Euler equations for the three conserved fields describe, in a suitable regime, the hydrodynamics of a one-dimensional fluid of interacting particles. At the level of the Euler equations there is no entropy increase. While this is well known, we provide an argument for it here, since we will need to refer to the argument later. So consider the one-dimensional Euler equations:

$$\partial_t \rho + \partial_x (\rho v) = 0, \quad (18a)$$

$$\partial_t (\rho v) + \partial_x (\rho v^2 + P) = 0, \quad (18b)$$

$$\partial_t \left( \rho \tilde{e} + \frac{1}{2} \rho v^2 \right) + \partial_x \left[ v \left( \rho \tilde{e} + \frac{1}{2} \rho v^2 + P \right) \right] = 0, \quad (18c)$$

where  $\tilde{e}(x, t) = e/\rho - v^2/2$  (Note:  $\epsilon$  is the internal energy density and  $\tilde{e} = \epsilon/\rho$ ) is the internal energy per particle and the pressure, for an ideal gas system is given by  $P =$

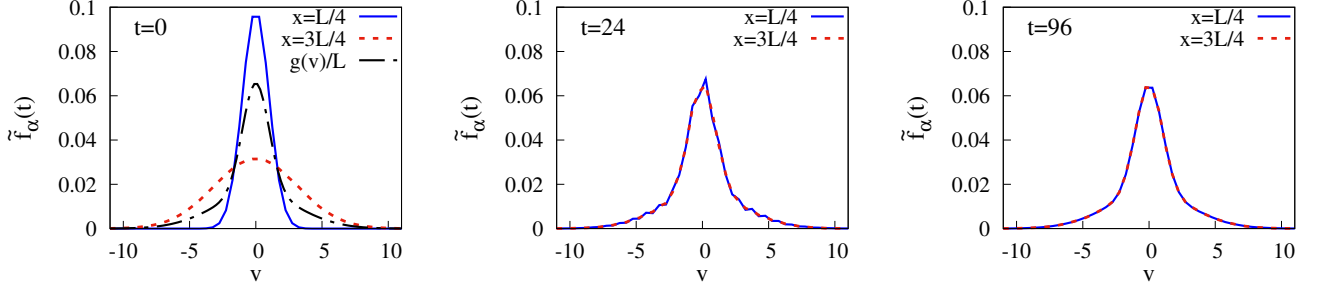


FIG. 8. Plot of evolution of the empirical particle density  $\tilde{f}_\alpha(x, v, t) = f_\alpha(x, v, t)/N$ , starting from a single two-temperature initial microstate, at two spatial locations  $x = L/4$  and  $x = 3L/4$ . The initial position of  $N = 10^7$  particles are distributed uniformly within  $(0, L)$  with  $L = 4$ , while the initial velocities of the particles in the left and right halves are drawn from Maxwell distributions at temperatures  $T_L = 1$  and  $T_R = 10$ , respectively. The grid size was taken as  $\Delta x = \Delta v = 0.5$ . At  $t = 0$  the empirical density  $f_\alpha(x, v, t)$  is Maxwellian with  $T_0 = 1$  and  $T_0 = 10$  at  $x = L/4$  and  $x = 3L/4$ , respectively. As time evolves, the empirical density at any position gets contribution from particles originating initially from both the Maxwell distributions. After a large time, the distribution  $f_\alpha(x, v, t)$  is seen to approach the form  $g(v)/L$  (shown by the black dash-dot line in the left-most panel), where  $g(v) = [g_{\text{eq}}(v, 1) + g_{\text{eq}}(v, 10)]/2$  and  $g_{\text{eq}}(v, T_0)$  is given in Eq. (17).

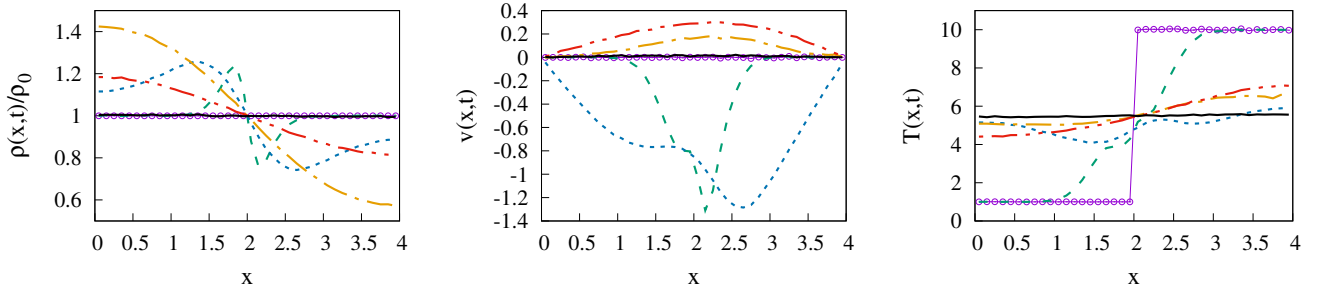


FIG. 9. Plot of the spatial profiles of the three conserved fields density  $\rho(x, t)$ , velocity  $v(x, t)$ , and temperature  $T(x, t)$  for the ‘two-temperature case’ at different times  $t = 0$  (magenta circles),  $0.1$  (green dashed lines),  $0.4$  (blue dotted lines),  $1$  (yellow dash-dot lines),  $2$  (red dash-dot-dot lines), and  $4$  (black solid lines) obtained from simulation of a single initial microscopic configuration with  $N = 10^7$  particles. The initial condition is the same as that used in Fig. 8. Notice that after a highly nontrivial evolution, all three profiles become flat and thus the system reaches the equilibrium state at long times.

$\rho T$ . These equations can be written in the form

$$\frac{D\rho}{Dt} + \rho \partial_x v = 0, \quad (19a)$$

$$\frac{Dv}{Dt} + \frac{1}{\rho} \partial_x P = 0, \quad (19b)$$

$$\frac{D\tilde{E}}{Dt} + \frac{1}{\rho} P \partial_x v = 0, \quad (19c)$$

where  $D/Dt = \partial_t + v\partial_x$  denotes the advective derivative. Now we use the Euler hydrodynamic equations along with Clausius’ laws of thermodynamics to determine the entropy production rate in the slowly evolving local equilibrium state. Clausius’ laws of thermodynamics provide a well-known thermodynamic relation for the ideal gas, given by  $TdS = d\tilde{E} + PdL$ , where  $S$  is the Clausius entropy,  $\tilde{E}$  is total internal energy and  $L$  is the volume. Applying this relation to a small volume  $\ell$  with a fixed number of particles  $n_\ell$  we find, after some manip-

ulations,

$$Tds = d\tilde{E} + Pd(\ell/n_\ell),$$

$$\text{hence, } \frac{Ds}{Dt} = \frac{1}{T} \left[ \frac{D\tilde{E}}{Dt} - \frac{P}{\rho^2} \frac{D\rho}{Dt} \right],$$

with  $s(x, t)$  being the entropy per particle. From Eqs. (19a) and (19c) we then immediately obtain that  $\frac{Ds}{Dt} = 0$ . The total entropy  $S(t) = \int_0^L \rho s(x, t) dx$  also remains constant, since  $dS/dt = - \int_0^L dx \partial_x(\rho vs) = 0$ , using the boundary conditions  $v(0, t) = v(L, t) = 0$ . The standard mechanisms of entropy growth in the hydrodynamic description are either additional dissipative (Navier-Stokes-Fourier) terms or the formation of shocks.

We now discuss entropy production in our non-interacting gas using a similar description, keeping in mind that we now do not expect a closed set of hydrodynamic equations with the three fields. In fact it is easy to see that the first two Euler equations in Eqs. (18) continue to hold while the equation for the energy field

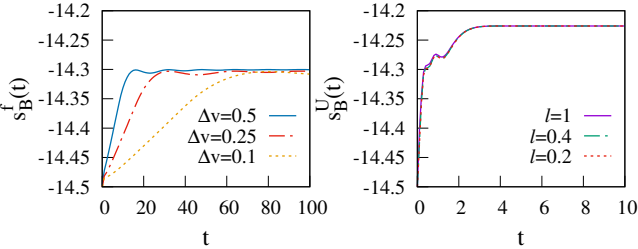


FIG. 10. Plot of  $s_B^f(t)$  and  $s_B^U(t)$  obtained from simulation of a single realization starting from the two-temperature initial configuration. The initial condition is the same as that used in Fig. 8. We have used several grid sizes for computing  $s_B^f$  and  $s_B^U$ . While both entropies saturate at large times, only the final value of  $s_B^U$  corresponds to the thermodynamic equilibrium value. Since the final velocity distribution at long times is not Maxwellian, the saturation value of  $s_B^f$  does not correspond to the equilibrium value. Observe that the growth is non-monotonic in both cases. We also see convergence of  $s_B^U$  with coarse-graining scale  $\ell$  while for  $s_B^f$  we again see a decreasing growth rate with decreasing  $\Delta v$ .

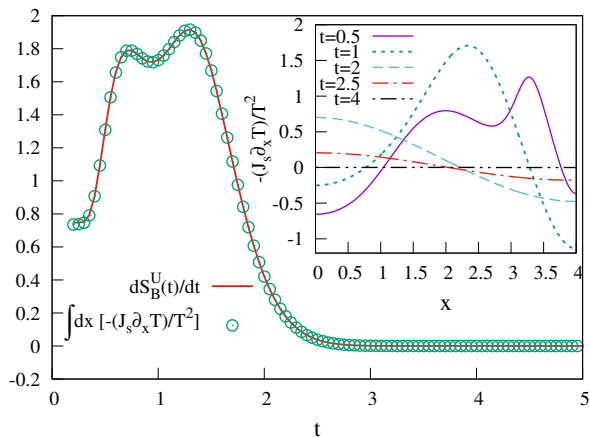


FIG. 11. Verification of entropy production rate as in Fig. 5 using Eq. (24). The red line is the LHS of Eq. (24) where  $S_B^U(t)$  is calculated from the definition given by Eq. (15) and the green points are the RHS of Eq. (24) calculated from hydrodynamics. Inset: Plot of the integrand in Eq. (24) with space  $x$  at different times.

$e(x, t)$  no longer holds. Formally the energy field satisfies the exact conservation equation

$$\partial_t e + \partial_x J = 0, \quad (20)$$

$$\text{where } J(x, t) = \frac{1}{2} \int_{-\infty}^{\infty} dv v^3 f(x, v, t). \quad (21)$$

is the energy current density. It is instructive to rewrite this equation in the following form:

$$\partial_t e + \partial_x [v(e + P)] = -\partial_x J_s, \quad (22)$$

$$\text{where } J_s(x, t) = J - v(e + P) \quad (23)$$

is the current after subtracting the reversible Euler part. This current,  $J_s$ , can be interpreted as a “heat” current. Then, repeating the steps as before we find that the entropy production rate is finite and given by

$$\frac{dS(t)}{dt} = - \int_0^L dx \frac{\partial_x J_s}{T} = - \int_0^L dx \frac{J_s \partial_x T}{T^2}, \quad (24)$$

where in the last step we used the fact that the current vanishes at the boundaries. For our system we can compute the fields  $J_s(x, t)$  and  $T(x, t)$  directly from the exact solution of the microscopic dynamics and thereby compute the entropy production rate from the above equation. In Fig. 11 we compare this with the entropy production rate obtained from the definition given by Eq. (15) and find perfect agreement between the two. However, as shown in the inset of Fig. 11, we find that the integrand is not everywhere non-negative and we are not able to prove analytically that the entropy production rate is non-negative. Note that for generic interacting non-integrable systems, the term  $J_s$  should be expressible in terms of the three basic fields and in fact given by the Fourier’s law  $J = -\kappa \partial_x T$ . This form would then guarantee non-negativity of the entropy production rate.

## VI. GEOMETRICAL OVERVIEW

Apart from the macrovariables,  $U, f$ , let us also define another one, corresponding to the global velocity distribution:  $g(v) = \int dx f(x, v)$ . For the equal mass gas, this is a constant of the motion. Each of  $U$ ,  $f$  and  $g$  define partitions of  $\Gamma_E$ :  $\Gamma_E = \{\Gamma_U\} = \{\Gamma_f\} = \{\Gamma_g\}$ , where  $\{\dots\}$  represents the collection of all possible macrostate values. The last,  $\{\Gamma_g\}$ , is a partition of  $\Gamma_E$  into sets invariant under the dynamics. Each of the three partitions has a dominant set,  $\Gamma_{U_{\text{eq}}}$ ,  $\Gamma_{f_{\text{eq}}}$ , and  $\Gamma_{g_{\text{eq}}}$ , respectively. These are shown schematically in Fig. 12. The macrostate  $U_{\text{eq}}$  corresponds to uniform profiles of the conserved fields,  $f_{\text{eq}}$  corresponds to a macrostate with uniform density profile and Maxwellian velocity distribution, and  $g_{\text{eq}}$  corresponds to a global Maxwellian velocity distribution. Note that the  $f$  partition of  $\Gamma_E$  is a refinement of the  $U$  partition and also a refinement of the  $g$  partition.

As shown in the figure,  $\Gamma_{f_{\text{eq}}}$  is the dominant set in  $\Gamma_{U_{\text{eq}}}$  and in  $\Gamma_{g_{\text{eq}}}$ , while  $\Gamma_{g_{\text{eq}}}$  has tiny regions that are outside  $\Gamma_{U_{\text{eq}}}$  and vice-versa. Any initial microstate,  $X_1(0)$ , inside  $\Gamma_{g_{\text{eq}}}$ , such as the one chosen from thermal equilibrium in the left half of the box, will eventually be in the region  $\Gamma_{f_{\text{eq}}} \cap \Gamma_{U_{\text{eq}}} \cap \Gamma_{g_{\text{eq}}} = \Gamma_{f_{\text{eq}}}$  which corresponds to “complete” thermal equilibrium. On the other hand typical microstates such as  $X_3(0)$ , chosen from outside of  $\Gamma_{g_{\text{eq}}}$ , will end in  $\Gamma_{U_{\text{eq}}}$  but outside  $\Gamma_{f_{\text{eq}}}$  and so in this case we have restricted thermalization. This is seen in Fig. 10 where  $s_B^U$  is seen to reach its equilibrium value while  $s_B^f$  does not. Finally one has very special atypical microstates,  $X_2(0)$ , such as in the alternate velocity case considered in Fig. 7, which remains outside  $\Gamma_{f_{\text{eq}}} \cup \Gamma_{U_{\text{eq}}} \cup \Gamma_{g_{\text{eq}}}$  and

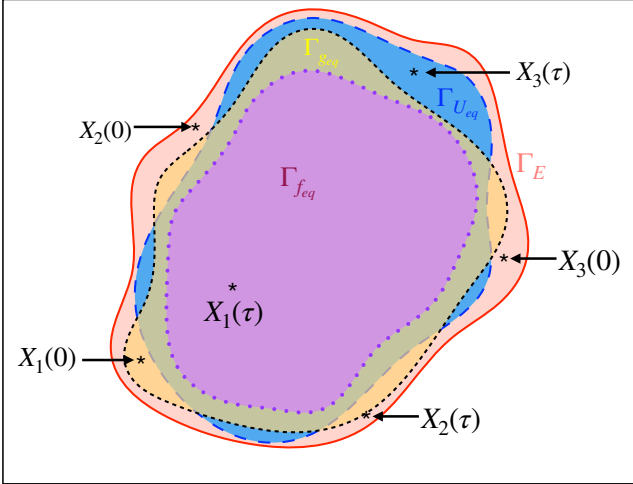


FIG. 12. A schematic showing the partition of the full phase space into subspaces defined by the equilibrium macrostates  $f_{eq}$  (boundary shown by dotted-line),  $U_{eq}$  (boundary with long-dashed line) and  $g_{eq}$  (boundary with dashed line). The points  $X_1(0), X_2(0), X_3(0)$  correspond to the three initial microstates considered in our study. The point  $X_1(0)$  corresponds to the free expansion from thermal equilibrium,  $X_2(0)$  corresponds to free expansion from the alternate velocity microstate and  $X_3(0)$  corresponds to the uniform density non-Maxwellian (two-temperature) initial global velocity distribution. After a long time,  $\tau$ , these microstates,  $X_1(\tau), X_2(\tau), X_3(\tau)$ , would remain in regions of phase space as shown in the figure (making brief excursions out of these regions on Poincare recurrence time-scales). We note that  $X_1(\tau)$  will be contained in  $\Gamma_{f_{eq}}$ ,  $X_2(\tau)$  is outside  $\Gamma_{f_{eq}} \cup \Gamma_{U_{eq}} \cup \Gamma_{g_{eq}}$ , and  $X_3(\tau)$  will end up in  $\Gamma_{U_{eq}} \setminus \Gamma_{f_{eq}}$  (all points in  $\Gamma_{U_{eq}}$  that are not in  $\Gamma_{f_{eq}}$ ).

there is no thermalization at all. The above features are specific to our system, a non-interacting integrable model. For non-integrable models it is expected that almost any initial microstate would end in  $\Gamma_{f_{eq}}$  and the system would thermalize completely.

## VII. CONCLUSION

In this paper, we have studied entropy increase during the free expansion of an ideal gas. In the microscopic description we start from an initial condition where the molecules are uniformly distributed in the left half of a box and the velocities are chosen from a thermal distribution. For this system we study the evolution of the Boltzmann entropy defined for a single microstate with two choices of macrovariables: the empirical single particle distribution  $f(x, v, t)$  and the profiles of density, momentum and energy  $U = [\rho(x), p(x), e(x)]$  (or equivalently  $\rho, v, T$ ). The corresponding entropies are  $s_B^f$  and  $s_B^U$ , respectively. In equilibrium, both these choices correspond to the thermodynamic entropy  $S$ . We summarize here our main findings:

- The time evolution of the empirical density  $f(x, v, t)$  and the fields  $\rho(x, t), v(x, t), T(x, t)$  were obtained for a single realization, starting from a single typical initial microstate chosen from the equilibrium macrostate where all particles are in equilibrium in the left half of a box. We found that these agree, in the large  $N$  limit, with the corresponding fields  $F_\alpha, \bar{\rho}, \bar{v}, \bar{T}$ , obtained by *averaging* over initial microstates taken from the relevant initial Gibbs distribution or, more or less equivalently, from the same initial macrostate. For our model, the averaged fields can easily be computed exactly, using Jepsen's [22] mapping to non-interacting particles. This thus demonstrate that the evolution of the macrostates and the corresponding entropies, for single typical microstates (belonging to a macrostate  $M_{ini}$ ), agrees with the evolution obtained after averaging over the ensemble of initial conditions (corresponding to the same initial macrostate  $M_{ini}$ ).

- Both  $s_B^f$  and  $s_B^U$  increase with time and eventually reach the expected equilibrium value with an increase of  $\ln(2)$  per particle. However, while  $s_B^U$  increases monotonically with time,  $s_B^f$  oscillates. The oscillations can be understood when one realizes that this system can be mapped to a non-interacting gas.
- The entropies are defined in terms of coarse graining scales  $|\Delta_\alpha|$  for  $s_B^f$  and  $\ell$  for  $s_B^U$ . We find that the entropy production rate for  $s_B^f$  decreases with decreasing grid-size  $|\Delta_\alpha|$  whereas for  $s_B^U$  we find that the entropy production rate does not depend much on decreasing grid-size  $\ell$ . We note that for any finite grid sizes, the empirical densities as well as the associated entropies eventually reach the equilibrium values (corresponding to the equilibrium macrostate of particles in the full box).
- Finally we show that the entropy increase for  $s_B^U$  can be related to a microscopic “heat” current,  $J_s$ , and formally the local entropy production rate can be written in the form  $J_s \partial_x (1/T)$ . However, we find that this is not positive-definite (as expected for non-integrable systems with heat diffusion). Nevertheless, the integral over all space gives a positive entropy production.
- **Other initial conditions:** The results above are for the specific case of free expansion. We have also studied other initial conditions. We considered one example (with an atypical initial microstate with alternate particles having different velocities,  $\pm v_0$ ) where the system never reaches a steady state and the entropy shows persistent oscillations. Our second example involves particles initially distributed uniformly in the box but with a non-Maxwellian global velocity distribution. For this case we find that  $s_B^U$  saturates to its equilibrium value at long

times, while  $s_B^f$  does not, corresponding to the observed fact that the macrovariables  $f$  and  $U$  evolve in this case to limiting values:  $U$  evolves to its equilibrium value  $U_{\text{eq}}$  while  $f$  evolves to  $g/L$ , corresponding to the dominant  $f$ -macrostate given the total velocity distribution arising from  $f_{\text{initial}}$ .

Our study illustrates the crucial role of coarse-graining, which leads to entropy increase, irreversibility and approach to thermal equilibrium, even in a non-interacting integrable system. Our results also highlight the importance of the choice of the macrovariables, in order to observe the monotonic growth of entropy, as has been discussed earlier for the case of dense fluids [20].

Thus we conclude that typicality, large numbers and coarse-graining play an important role in explaining irreversibility in macroscopic dynamics and entropy increase, whereas, the ideas of ergodicity, interaction and chaos are not essential. It will be interesting to extend this study to interacting systems also such as the alternate mass hard particle gas (AMHPG) where the masses of alternate particles take different values. This non-integrable model has been studied extensively in the context of the breakdown of Fourier's law of heat conduction in one dimension [36–39] and verification of the hydrodynamic description [40–43]. For this case we expect important differences from the present integrable model even though

the equilibrium thermodynamics of both are identical. For example we expect that the entropy production rate for  $s_B^f$  at a fixed time should converge to a finite positive value even in the limit of vanishing grid-size, in contrast to what we see in Fig. 2. Another difference is that we expect is that the heat current term,  $J_s$ , in Eq. (23) should be given by Fourier's law leading to positive entropy production rate at the local level (in contrast to the inset in Fig. 11).

## ACKNOWLEDGMENTS

SC, AD and AK acknowledge support of the Department of Atomic Energy, Government of India, under Project No. RTI4001 and would also like to acknowledge the ICTS program on “Thermalization, Many body localization and Hydrodynamics (Code:ICTS/hydrodynamics2019/11)” for enabling crucial discussions related to this work. SC, AD and AK thank Cedric Bernardin, Deepak Dhar, Francois Huveneers, Christian Maes, Stefano Olla, and Herbert Spohn for illuminating discussions. The work of JLL was supported by the AFOSR. The numerical simulations were performed on a Mario HPC at ICTS-TIFR.

- 
- [1] L. Boltzmann, On Zermelo's paper “On the mechanical explanation of irreversible processes”, *Annalen der Physik* **60**, 392 (1897).
- [2] R. Feynman, *The character of physical law* (MIT press, 2017).
- [3] O. E. Lanford, On a derivation of the Boltzmann equation, *Astérisque* **40**, 117 (1976).
- [4] R. Penrose, *The Emperor's New Mind: Concerning Computers, Minds, and the Laws of Physics* (Oxford University Press, Inc., USA, 1989).
- [5] B. Greene, *The fabric of the cosmos: Space, time, and the texture of reality* (Knopf, 2004).
- [6] J. L. Lebowitz, Macroscopic laws, microscopic dynamics, time's arrow and Boltzmann's entropy, *Physica A: Statistical Mechanics and its Applications* **194**, 1 (1993).
- [7] J. L. Lebowitz, Boltzmann's entropy and time's arrow, *Physics Today* **46**, 32 (1993).
- [8] J. L. Lebowitz, From time-symmetric microscopic dynamics to time-asymmetric macroscopic behavior: An overview, in *Boltzmann's Legacy (ESI Lectures in Mathematics and Physics)*, edited by G. Gallavotti, W. L. Reiter, and J. Yngvason (European Mathematical Society, 2008) p. 63, arXiv:0709.0724 [cond-mat.stat-mech].
- [9] S. Goldstein, J. L. Lebowitz, R. Tumulka, and N. Zanghì, Gibbs and Boltzmann entropy in classical and quantum mechanics, in *Statistical Mechanics and Scientific Explanation: Determinism, Indeterminism and Laws of Nature*, edited by V. Allori (World Scientific, Singapore, 2020) Chap. 14, p. 519, arXiv:1903.11870 [cond-mat.stat-mech].
- [10] J. L. Lebowitz, Statistical mechanical ensembles and typical behavior of macroscopic systems, (Talk at ICTS, 2021).
- [11] H. Tasaki, Typicality of thermal equilibrium and thermalization in isolated macroscopic quantum systems, *Journal of Statistical Physics* **163**, 937 (2016).
- [12] T. Mori, T. N. Ikeda, E. Kaminishi, and M. Ueda, Thermalization and prethermalization in isolated quantum systems: a theoretical overview, *Journal of Physics B: Atomic, Molecular and Optical Physics* **51**, 112001 (2018).
- [13] J. Orban and A. Bellemans, Velocity-inversion and irreversibility in a dilute gas of hard disks, *Physics Letters A* **24**, 620 (1967).
- [14] D. Levesque and L. Verlet, Molecular dynamics and time reversibility, *Journal of Statistical Physics* **72**, 519 (1993).
- [15] V. Romero-Rochín and E. González-Tovar, Comments on some aspects of Boltzmann  $H$  theorem using reversible molecular dynamics, *Journal of Statistical Physics* **89**, 735 (1997).
- [16] B. T. Nadiga, J. E. Broadwell, and B. Sturtevant, Study of a multispeed cellular automaton, in *Rarefield Gas Dynamics: Theoretical and Computational Techniques*, Vol. 118, edited by E. P. Muntz, D. P. Weaver, and D. H. Campbell (American Institute of Aeronautics and Astronautics, Washington, DC, 1989) Chap. 2, p. 155.
- [17] M. Falcioni, L. Palatella, S. Pigolotti, L. Rondoni, and A. Vulpiani, Initial growth of Boltzmann entropy and chaos in a large assembly of weakly interacting systems, *Physica A: Statistical Mechanics and its Applications* **385**, 170 (2007).

- [18] E. T. Jaynes, Violation of Boltzmann's  $H$  theorem in real gases, *Phys. Rev. A* **4**, 747 (1971).
- [19] S. Goldstein and J. L. Lebowitz, On the (Boltzmann) entropy of non-equilibrium systems, *Physica D: Nonlinear Phenomena* **193**, 53 (2004).
- [20] P. L. Garrido, S. Goldstein, and J. L. Lebowitz, Boltzmann entropy for dense fluids not in local equilibrium, *Phys. Rev. Lett.* **92**, 050602 (2004).
- [21] H. L. Frisch, Poincaré recurrences, *Phys. Rev.* **104**, 1 (1956).
- [22] D. Jepsen, Dynamics of a simple many-body system of hard rods, *Journal of Mathematical Physics* **6**, 405 (1965).
- [23] J. L. Lebowitz and J. K. Percus, Kinetic equations and density expansions: Exactly solvable one-dimensional system, *Phys. Rev.* **155**, 122 (1967).
- [24] J. L. Lebowitz, J. K. Percus, and J. Sykes, Time evolution of the total distribution function of a one-dimensional system of hard rods, *Phys. Rev.* **171**, 224 (1968).
- [25] J. K. Percus, Exact solution of kinetics of a model classical fluid, *The Physics of Fluids* **12**, 1560 (1969).
- [26] A. Roy, O. Narayan, A. Dhar, and S. Sabhapandit, Tagged particle diffusion in one-dimensional gas with hamiltonian dynamics, *Journal of Statistical Physics* **150**, 851 (2013).
- [27] A. Kundu and A. Dhar, Equilibrium dynamical correlations in the toda chain and other integrable models, *Phys. Rev. E* **94**, 062130 (2016).
- [28] C. Boldrighini, R. L. Dobrushin, and Y. M. Sukhov, One-dimensional hard rod caricature of hydrodynamics, *Journal of Statistical Physics* **31**, 577 (1983).
- [29] B. Doyon and H. Spohn, Dynamics of hard rods with initial domain wall state, *Journal of Statistical Mechanics: Theory and Experiment* **2017**, 073210 (2017).
- [30] X. Cao, V. B. Bulchandani, and J. E. Moore, Incomplete thermalization from trap-induced integrability breaking: Lessons from classical hard rods, *Phys. Rev. Lett.* **120**, 164101 (2018).
- [31] S. Goldstein, Individualist and ensemplist approaches to the foundations of statistical mechanics, *The Monist* **102**, 439 (2019).
- [32] S. Goldstein, D. A. Huse, J. L. Lebowitz, and R. Tumulka, Macroscopic and microscopic thermal equilibrium, *Annalen der Physik* **529**, 1600301 (2017).
- [33] S. Goldstein, D. A. Huse, J. L. Lebowitz, and P. Sartori, On the nonequilibrium entropy of large and small systems, in *Stochastic Dynamics Out of Equilibrium (IHPStochDyn 2017: Stochastic Dynamics Out of Equilibrium)*, Vol. 282, edited by G. Giacomin, S. Olla, E. Saada, H. Spohn, and G. Stoltz (Springer, Berlin, 2019) Chap. 22, p. 581, arXiv:1712.08961 [cond-mat.stat-mech].
- [34] S. Goldstein, Boltzmann's approach to statistical mechanics, in *Chance in Physics: Foundations and Perspectives (Lecture Notes in Physics)*, Vol. 574, edited by J. Bricmont, G. Ghirardi, D. Dürr, F. Petruccione, M. C. Galavotti, and N. Zanghì (Springer, Berlin, 2001) Chap. 3, p. 39, arXiv:0105242 [cond-mat.stat-mech].
- [35] M. Kardar, *Statistical Physics of Particles* (Cambridge University Press, 2007).
- [36] A. Dhar, Heat conduction in a one-dimensional gas of elastically colliding particles of unequal masses, *Phys. Rev. Lett.* **86**, 3554 (2001).
- [37] P. Grassberger, W. Nadler, and L. Yang, Heat conduction and entropy production in a one-dimensional hard-particle gas, *Phys. Rev. Lett.* **89**, 180601 (2002).
- [38] G. Casati and T. Prosen, Anomalous heat conduction in a one-dimensional ideal gas, *Phys. Rev. E* **67**, 015203 (2003).
- [39] P. Cipriani, S. Denisov, and A. Politi, From anomalous energy diffusion to levy walks and heat conductivity in one-dimensional systems, *Phys. Rev. Lett.* **94**, 244301 (2005).
- [40] H. Spohn, Nonlinear fluctuating hydrodynamics for anharmonic chains, *Journal of Statistical Physics* **154**, 1191 (2014).
- [41] C. B. Mendl and H. Spohn, Shocks, rarefaction waves, and current fluctuations for anharmonic chains, *Journal of Statistical Physics* **166**, 841 (2016).
- [42] S. Chakraborti, S. Ganapa, P. L. Krapivsky, and A. Dhar, Blast in a one-dimensional cold gas: From newtonian dynamics to hydrodynamics, *Phys. Rev. Lett.* **126**, 244503 (2021).
- [43] S. Ganapa, S. Chakraborti, P. Krapivsky, and A. Dhar, Blast in the one-dimensional cold gas: Comparison of microscopic simulations with hydrodynamic predictions, *Physics of Fluids* **33**, 087113 (2021).
- [44] H. L. Frisch, An approach to equilibrium, *Phys. Rev.* **109**, 22 (1958).

#### Appendix A: Exact solution for the evolution of macroscopic fields

Here we present exact results for the evolution of average fields corresponding to the empirical densities  $f(x, p, t)$  and  $[\rho(x, t), p(x, t), e(x, t)]$ . A similar study on a ring was done earlier in [44].

The mean density  $\bar{\rho}(x, t)$ , momentum  $\bar{p}(x, t)$  and energy  $\bar{e}(x, t)$  fields are defined as

$$\bar{\rho}(x, t) = \left\langle \sum_{j=1}^N \delta(x_j - x) \right\rangle_{\mathbf{x}_0, \mathbf{v}_0} = \int dv F(x, v, t), \quad (A1)$$

$$\bar{p}(x, t) = \left\langle \sum_{j=1}^N \delta(x_j - x) v_j \right\rangle_{\mathbf{x}_0, \mathbf{v}_0} = \int dv v F(x, v, t), \quad (A2)$$

$$\bar{e}(x, t) = \left\langle \sum_{j=1}^N \delta(x_j - x) \frac{v_j^2}{2} \right\rangle_{\mathbf{x}_0, \mathbf{v}_0} = \int dv \frac{v^2}{2} F(x, v, t). \quad (A3)$$

Here  $\langle \dots \rangle_{\mathbf{x}_0, \mathbf{v}_0}$  denotes an average over the initial positions and velocities,  $\mathbf{x}_0$  and  $\mathbf{v}_0$  respectively, of all the particles, which are chosen from the canonical distribution at temperature  $T_0$  with all particles in the left half  $(0, L/2)$ . In the following, we study the evolution of these fields in time and space for this system with two reflecting boundaries at  $x = 0$  and  $x = L$ .

The canonical ensemble implies that we distribute the particles uniformly in  $(0, L/2)$  and draw their velocities

from the Maxwell's velocity distribution given by

$$g_{\text{eq}}(v_0, T_0) = \left( \frac{1}{2\pi T_0} \right)^{1/2} \exp \left[ \frac{-v_0^2}{2T_0} \right]. \quad (\text{A4})$$

As discussed earlier, we can effectively treat the particles

as non-interacting and the problem reduces to a single particle problem [26]. We then consider a single particle starting from an initial position  $x_0$  with initial velocity  $v_0$ . The final position,  $x_t$ , of the particle, taking all possible collisions into account, can take the following forms:

$$x_t = \begin{cases} x_0 + |v_0|t - 2nL = x_0 + v_0t - 2nL, & \text{if } v_0 > 0, v_t > 0, \\ x_0 - |v_0|t + 2nL = x_0 + v_0t + 2nL, & \text{if } v_0 < 0, v_t < 0, \\ -x_0 - |v_0|t + 2nL = -x_0 - v_0t + 2nL, & \text{if } v_0 > 0, v_t < 0, \\ -x_0 + |v_0|t - 2nL = -x_0 - v_0t - 2nL, & \text{if } v_0 < 0, v_t > 0, \end{cases} \quad (\text{A5})$$

where  $v_t$ , the velocity at time  $t$ , can take either values  $\pm v_0$  and  $n = 0, 1, 2, 3, \dots$ , is the number of collision(s) that the particle has with both the boundaries. The distribution  $F(x, v, t)$  is then obtained by averaging over the initial position [uniform in  $(0, L/2)$ ] and velocity [drawn from  $g(v_0)$ ]:

$$F(x, v, t) = N \langle \delta(x - x_t) \delta(v - v_t) \rangle_{x_0, v_0}. \quad (\text{A6})$$

Using Eq. (A5) we get

$$F(x, v, t) = \frac{2N}{L} \int_0^{L/2} dx_0 \int_{-\infty}^{\infty} dv_0 g_{\text{eq}}(v_0) \sum_{n=-\infty}^{\infty} [\delta(x - x_0 - v_0 t + 2nL) \delta(v - v_0) + \delta(x + x_0 + v_0 t - 2nL) \delta(v + v_0)], \quad (\text{A7})$$

$$\begin{aligned} &= 2\rho_0 \frac{\exp(-v^2/2T)}{\sqrt{2\pi T}} \sum_{n=-\infty}^{\infty} \left[ \int_{x-vt+2nL-L/2}^{x-vt+2nL} \delta(z) dz + \int_{x-vt-2nL}^{x-vt-2nL-L/2} \delta(z) dz \right], \\ &= 2\rho_0 \frac{\exp(-v^2/2T)}{\sqrt{2\pi T}} \sum_{n=-\infty}^{\infty} [\theta(x - vt + 2nL) - \theta(x - vt + 2nL - L/2) + \theta(x - vt - 2nL - L/2) - \theta(x - vt - 2nL)], \end{aligned} \quad (\text{A8})$$

where  $\rho_0 = N/L$ . Now we calculate the three mean fields by performing the integrals in Eqs. (A1), (A2), and (A3) to get

$$\begin{aligned} \bar{\rho}(x, t) &= \int_{-\infty}^{\infty} dv F(x, v, t), \\ &= 2\rho_0 \frac{1}{\sqrt{2\pi T}} \sum_{n=-\infty}^{\infty} \int_0^{L/2} dx_0 \int_{-\infty}^{\infty} dv e^{-v^2/2T} [\delta(x - x_0 - vt + 2nL) + \delta(x + x_0 - vt - 2nL)], \\ &= 2\rho_0 \frac{1}{\sqrt{2\pi T}} \sum_{n=-\infty}^{\infty} \int_0^{L/2} dx_0 \frac{1}{t} \left[ \exp \left\{ \frac{-(2nL + x - x_0)^2}{2Tt^2} \right\} + \exp \left\{ \frac{-(2nL - x - x_0)^2}{2Tt^2} \right\} \right], \\ &= \rho_0 \sum_{n=-\infty}^{\infty} \left[ \text{erf} \left( \frac{L/2 - 2nL - x}{\sqrt{2Tt}} \right) + \text{erf} \left( \frac{L/2 - 2nL + x}{\sqrt{2Tt}} \right) \right]. \end{aligned} \quad (\text{A9})$$

Using the Poisson resummation formula, this can be rewritten in the alternative series form:

$$\bar{\rho}(x, t) = \rho_0 + 4\rho_0 \sum_{k=1}^{\infty} \frac{1}{k\pi} \sin \left( \frac{k\pi}{2} \right) \cos \left( \frac{k\pi x}{L} \right) \exp \left( \frac{-k^2\pi^2 T t^2}{2L^2} \right). \quad (\text{A10})$$

Following a similar approach we obtain the following expressions for the mean momentum and energy:

$$\begin{aligned}\bar{p}(x, t) &= \int_{-\infty}^{\infty} dv \, v F(x, v, t), \\ &= \rho_0 \sqrt{\frac{2T}{\pi}} \sum_{n=-\infty}^{\infty} \left[ -\exp \left\{ -\frac{(2nL+x)^2}{2Tt^2} \right\} + \exp \left\{ -\frac{(2nL-L/2+x)^2}{2Tt^2} \right\} + \exp \left\{ -\frac{(2nL-x)^2}{2Tt^2} \right\} \right. \\ &\quad \left. - \exp \left\{ -\frac{(2nL-L/2-x)^2}{2Tt^2} \right\} \right],\end{aligned}\tag{A11}$$

$$= \frac{4\rho_0 T t}{L} \sum_{k=1}^{\infty} \sin \left( \frac{k\pi}{2} \right) \sin \left( \frac{k\pi x}{L} \right) \exp \left( \frac{-k^2 \pi^2 T t^2}{2L^2} \right),\tag{A12}$$

$$\begin{aligned}\bar{e}(x, t) &= \frac{1}{2} \int_{-\infty}^{\infty} dv \, v^2 F(x, v, t), \\ &= \rho_0 \frac{2T}{\sqrt{\pi}} \sum_{n=-\infty}^{\infty} \left[ -\frac{2nL-x}{2\sqrt{2Tt}} \exp \left\{ \frac{-(2nL-x)^2}{2Tt^2} \right\} - \frac{2nL+x}{2\sqrt{2Tt}} \exp \left\{ \frac{-(2nL+x)^2}{2Tt^2} \right\} \right. \\ &\quad - \sqrt{\frac{\pi}{4}} \operatorname{erf} \left( \frac{2nL-L/2+x}{\sqrt{2Tt}} \right) + \frac{2nL-L/2+x}{2\sqrt{2Tt}} \exp \left\{ \frac{-(2nL-L/2+x)^2}{2Tt^2} \right\} \\ &\quad \left. - \sqrt{\frac{\pi}{4}} \operatorname{erf} \left( \frac{2nL-L/2-x}{\sqrt{2Tt}} \right) + \frac{2nL-L/2-x}{2\sqrt{2Tt}} \exp \left\{ \frac{-(2nL-L/2-x)^2}{2Tt^2} \right\} \right].\end{aligned}\tag{A13}$$

$$= \frac{\rho_0 T}{2} + 2\rho_0 T \sum_{k=1}^{\infty} \frac{1}{k\pi} \left( 1 - \frac{k^2 \pi^2 T t^2}{L^2} \right) \sin \left( \frac{k\pi}{2} \right) \cos \left( \frac{k\pi x}{L} \right) \exp \left( \frac{-k^2 \pi^2 T t^2}{2L^2} \right).\tag{A14}$$

From Eqs. (A10, A12, A14) one can easily see that the approach to equilibrium has the long-time form  $e^{-at^2}$  with  $a = T\pi^2/(2L^2)$ .

---